Cellulose derived nitrogen and phosphorus co-doped carbon-based catalysts for catalytic reduction of p-nitrophenol

Xiong Xie [a,b], Jie Shi [a,b], Yuan Pu [a,b,]*, Zhiyong Wang [a,b], Liang-Liang Zhang [b], Jie-Xin Wang [a,b], Dan Wang [a,b,]*

[a] State Key Laboratory of Organic-Inorganic Composites, Beijing University of Chemical Technology, Beijing 100029, China
[b] Research Center of the Ministry of Education for High Gravity Engineering and Technology, Beijing University of Chemical Technology, Beijing 100029, China

GRAPHICAL ABSTRACT

ABSTRACT

The cellulose, which is one of the most abundant solid by-products of agriculture and forestry industry, has been successfully tested for the synthesis of nitrogen and phosphorus co-doped carbon-based metal-free catalysts (NPC) via freeze-drying the mixture of cellulose crystallite and ammonium phosphate, followed by annealing of the hydrogel under nitrogen atmosphere at 800 °C for 2 h. Different techniques including TEM, SEM, FTIR and XPS spectroscopy have been applied to characterize the as-prepared NPC, which presents flake-like morphology with N and P doping levels of 4.3 atom% and 10.66 atom%, respectively. The NPC exhibits excellent catalytic activity for the reduction of p-nitrophenol (p-NP). The turnover frequency (TOF) of the reduction of p-NP is as high as 2×10^{-5} mmol·mg^{-1}·min^{-1} and the apparent kinetic rate constant was calculated as 0.0394 min^{-1} at room temperature. The catalytic mechanism is proposed by combining the density functional theory calculation and analysis of the experimental results. These findings open up new possibilities of valorization for cellulose-based by-product and treatment of p-NP-based wastewater.

© 2020 Elsevier Inc. All rights reserved.

1. Introduction

The p-nitrophenol (p-NP), which was widely found in industrial wastewater, can cause potential damage to vital organs of a human body such as liver and kidneys even in trace amounts for its toxic, carcinogenic, and stimulating property [1,2]. However, it is the

main raw material for the production of its corresponding amino compound, *p*-aminophenol (*p*-AP), an important intermediate for chemical industry products such as synthetic dyes, pharmaceuticals, and pesticides [3]. Therefore, how to chemical transform of harmful substances *p*-NP to *p*-AP by green and sustainable routes has attracted much attention [4,5]. In the past few years, many metal-based materials have been used as high-efficiency catalysts for *p*-NP to *p*-AP, such as silver [6], gold [7] and ultrafine palladium nanoparticles, etc [8–11]. While, due to the problems of scarce reserves, inactivation of aggregation, and solid waste pollution, the use of metal-based catalysts in industrial still facing various limitations and challenges [12].

Carbon-based metal-free catalysts have recently shown attractive prospects in many fields [13,14]. Especially, their potential for replacing traditional metal-based catalysts in many catalytic reactions was considered to be one of the green and sustainable routes in industry production [15]. The catalytic activity of carbon-based materials is particularly relevant with the surface group types (—OH, —SO$_3$, and so on) and electronic arrangement state of carbon skeleton. That is, as a metal free heteroatoms (B, N, P, S, etc.) doping into the carbon skeleton can disorganize the high symmetry electron arrangement state of intrinsic carbon structure, the electronic activity was significantly improved, and thus result in high catalytic performance [16,17]. Particularly, co-doping with several different heteroatoms into the carbon skeleton can usually display dramatic performance for special electric redistribution caused by the synergistic effect between different heteroatoms [18]. Interestingly, cellulose, which is widely distributed and abundant polysaccharide in nature, can be used as a carbon source as more than 50% of carbon content in abandoned crops [19]. Although double-doped cellulosic carbon materials have been extensively studied in electrochemical catalysis [20,21], there hardly studies focusing on cellulose-based carbon catalysts for organic catalytic reactions. Although a variety of catalytic mechanisms have been proposed for metal-free catalytic systems by using a large number of theoretical simulations, the mechanisms for these reactions still have not been adequately verified, especially for diatomic doping catalysts. Therefore, the exploitation of an economic effective dual-doped cellulose-derived catalyst and its mechanism in organic catalysis remains a hugely difficult problem.

Here, we reported the preparation of nitrogen and phosphorus co-doped carbon (NPC) materials by directly annealing the homogenous mixture of α-cellulose crystallite and ammonium phosphate ((NH$_4$)$_2$HPO$_4$). Because of the synergistic effect of nitrogen and phosphorus heteroatoms doped in the carbon hexatomic ring skeleton, the as-prepared NPC catalyst exhibits an enhanced catalytic performance in *p*-NP reduction reaction. In addition, the catalytic reaction mechanism, as well as the energy change of each step in the reaction process, are explored by the thermodynamics experiment combined with density functional theory (DFT) calculations.

2. Materials and methods

2.1. 1. Preparation of NPC

10 g of α-cellulose crystallite and 50 mL of (NH$_4$)$_2$HPO$_4$ (1 M) solution were mixed in a beaker and sonicated for 6 h, after that, the mixture was freeze-drying overnight to remove water. Then the obtained solid particles were ground and directly annealed to 800 °C for 2 h with a heating rate of 10 °C min^{-1} under N$_2$ atmosphere. After cooling down to room temperature naturally, the obtained carbonized powder was washed by deionized water and ethanol for 3 times to remove the unreacted ammonium salts, and then dried in vacuum oven at 80 °C overnight.

For comparison, the synthesis of undoped annealed cellulose (UAC) was performed in the same method by using α-cellulose crystallite only. Metal is not involved in the whole process.

2.2. Characterization

The morphology of sample was characterized with transmission electron microscope (TEM) images, which were taken by Hitachi H-9500 high-resolution TEM operating in bright-field mode. Scanning electron microscopy (SEM) imaging and energydispersive X ray (EDX) mapping was performed on a Hitachi S-4700 field emission SEM. Fourier transform infrared (FTIR) spectra were measured on a Thermo Fisher Nicolet 6700 FTIR system. The X-ray diffraction (XRD) analysis was performed on a Shimadzu XRD-6000 diffractometer. X-ray photoelectron spectroscopy (XPS) measurements were performed on a VG Microtech ESCA 2000 instrument using a monochromic Al X-ray source.

2.3. Catalytic evaluation

The catalytic reduction of *p*-NP was evaluated using a modified literature procedure [22]. Typically, 30 mg of NPC catalysts were dispersed in 30 mL aqueous solution containing 1.5 mmol NaBH$_4$ and 0.015 mmol *p*-NP. To monitor the reaction process, 3.5 mL solution was transferred to a quartz cuvette. The absorption spectrum of each solution was measured at specific times (0–25 min, 5 min apart) by using a Shimadzu UV2600 UV–vis spectrometer. According to Beer-Lambert law, the concentrations of *p*-NP and *p*-AP were calculated from the absorbance at the peaks of 400 and 300 nm, respectively [23].

2.4. DFT simulation

First-principle calculations were performed on the Vienna ab initio simulation package (VASP.5.4.1) based on spin-polarized DFT [24]. The reparameterized of Perdew-Burke-Ernzerhof (revPBE) form of the generalized gradient approximation (GGA) was used to calculate nonlocal gradient corrections to the correlation and exchange energies [25,26]. The wave functions were constructed from the expansion of plane waves with an energy cutoff of 450 eV. The electron-ion interactions in the core region were described by Vanderbilt ultrasoft pseudopotentials with real space projection operators [27]. A $1 \times 1 \times 1$ Monkhorst-Pack k-point sampling in the Brillouin zone was performed for the cube cell of 20 Å length to avoid interactions between the periodic structures. For accuracy, the density of states (DOS) was calculated at the k-point of $5 \times 5 \times 1$. To simplify calculations, geometric optimization was performed using a graphitic carbon skeleton of 28 C atoms and 14 H atoms, in which one or two C atoms are replaced by N/P atom to represent N/P doped carbon materials. A tight convergence of 0.01 eV/Å on the forces with the wave functions converged to 1×10^{-5} eV was carried out. All calculations were performed using the Rutgers-Chalmers van der Waals Density Functional (vdw-DF) method to accurately describe the dispersion interactions between the adsorbate and adsorbent [28].

The NPC model considers that the N, P, and O elements have seven possible dopings in the carbon skeleton. The adsorption energy (E_{ads}) of the *p*-NP molecule on the surface of catalytic material was calculated according to Eq. (1).

$$E_{ads} = E_{total} - E_{catalyst} - E_{molecule} \tag{1}$$

where E_{total} is the total energy of the optimized system, $E_{catalyst}$ is the energy of the catalysts, and $E_{molecule}$ is the energy of the adsorbed molecule.

3. Results and discussion

The synthesis process of the NPC catalyst is shown in Fig. 1. Briefly, the carbon-based catalysts was achieved by soaking the α-cellulose crystallite in $(NH_4)_2HPO_4$ solution, followed by the freeze drying treatment and then annealing of the powder. The α-cellulose crystallite serves as a carbon source while $(NH_4)_2HPO_4$ supply nitrogen and phosphorus atoms for the doping process. Generally, the oxygen-containing groups (—OH, and —C—O—C) in α-cellulose crystallites would be destroyed at high temperature under inert gas atmosphere and causing recombination and carbonization reaction to generate defect carbon skeleton [29]. Then the unstable defect sites on the carbon skeleton will react with H_3PO_4 and NH_3 obtained from the decomposition of $(NH_4)_2HPO_4$ to form nitrogen and phosphorus co-doped carbon material.

The surface morphology and microstructure of the as-prepared NPC was investigated by scanning electron microscopy (SEM), and transmission electron microscopy (TEM), respectively. As shown in Fig. 2a, the NPC displays a graphene-like structure with transparent and ultra-thin nanosheets. Fig. 2b shows that the surface of the NPC is in wrinkled flake-like morphology. Moreover, as shown in Fig. 2c–g, the SEM corresponding EDX mapping images indicate that the carbon, nitrogen, and phosphorus elements are uniform distribute on the surface of carbon nanosheets, which verifying the successful doping of nitrogen and phosphorus elements [30,31].

The chemical bond type of NPC was measured by FTIR. As shown in Fig. 3a, the peaks at around 2961 cm^{-1}, 1734 cm^{-1}, 1614 cm^{-1}, and 1399 cm^{-1} correspond to C—H, C=O, C=C, and C—O stretching, respectively. Especially, NPC has an additional P—O stretching vibration (1087 cm^{-1}) and —PO$_4$ asymmetric stretching vibration (987 cm^{-1}) when compared with UAC. The abundant presence of oxygen-containing groups (—OH, P—O, —PO$_4$) also indicates that the hydrophilicity of NPC is much better than that of UAC (Fig. S1). In XRD pattern of UAC, the broad diffraction peak at around 24° is indexed to the amorphous carbon plane while the NPC shows a (0 0 2) plane of graphitic carbon diffraction peak at about 26° [13,32–38]. This angular migration demonstrates the formation of a graphitic structure, which attributed to the synergistic effect of nitrogen and phosphorus doping during graphitization [31,34].

The chemical structure of NPC is further investigated by the XPS spectrum, which shown in Fig. 4. The results reveal the distribution of C, O, P, and N with a proportion of 51.5%, 33.6%, 10.6%, and 4.3%,

respectively, indicating the formation of N and P dual-doping in the NPC (Fig. 4a). Furthermore, the high solution XPS of C 1s in NPC shown in Fig. 4b displays three kinds of carbon bonds in NPC, that is, graphite sp^2 C (284.74 eV), N-sp^2 C (285.88 eV), and C=O bond (288.9 eV) [31,32,37]. As shown in Fig. 4c, the N 1s spectra of NPC can be divided into three peaks at 398.5 eV, 399.6 eV, and 401.2 eV, which correspond to pyridinic N, pyrrolic N, and graphitic N, respectively [39]. For P 2p spectra, there are two peaks with P—C at 132.86 eV and P—O at 133.6 eV [31,38,40]. These results further demonstrate that the N and P atoms are incorporated into the carbon framework of the NPC (Fig. 4d) [40].

The hydrogenation of p-NP with excess sodium borohydride (NaBH$_4$), which is a typical organic catalytic reaction, was used to assess the catalytic performance of NPC. Firstly, 3.48 mg of p-NP crystal dissolved in 50 mL deionized (DI) water with sonication for 30 min, and the absorption peak of the original p-NP solution is about 318 nm detected by UV–visible spectrophotometer. Interestingly, the color of the solution changed from light yellow to bright yellow after 56.75 mg NaBH$_4$ powder added, also, the UV–vis characteristic peak moves from 310 to 400 nm. The changes in color and peak were owing to the formation of p-nitrophenolate [5,22]. However, without a catalyst, the peak of the newly prepared NaBH$_4$/p-NP mixture was consistent after placing for 7 days (Fig. S2). This phenomenon reveals that this reaction does not immediately happen in the absence of catalysts because of its high energy barrier [31]. When the NPC catalysts were added to NaBH$_4$/p-NP mixture solution, a large number of bubbles are rapidly generated (Fig. S3a), and the bright yellow color of the solution gradually changes to colorless, which can be one of the obvious signal of the reduction reaction happens [5,8,31]. In the meanwhile, the process of the reaction was monitor by UV–Vis, that is, the mixture solution was scanned every 5 min and the spectra were shown in Fig. 5a. Obviously, the concentration of p-NP decreased and the p-AP peak goes up gradually as the reaction proceeds. Under the same conditions, the UAC was used to catalyze the reduction of p-NP (Fig. S3b). It was found that the bright yellow color does not fade away and the UV–visible absorption peak of p-NP hardly changed without the appearance of p-AP characteristic peak even react for one week.

Fig. 5b displays that the ln (C/C_0) is linear dependent on the reaction time, indicating that the reduction of p-NP catalyzed by NPC follows pseudo-first-order kinetics with excess NaBH$_4$ [12,22,41]. The apparent rate constant, k_{app}, can be calculated as the following equation:
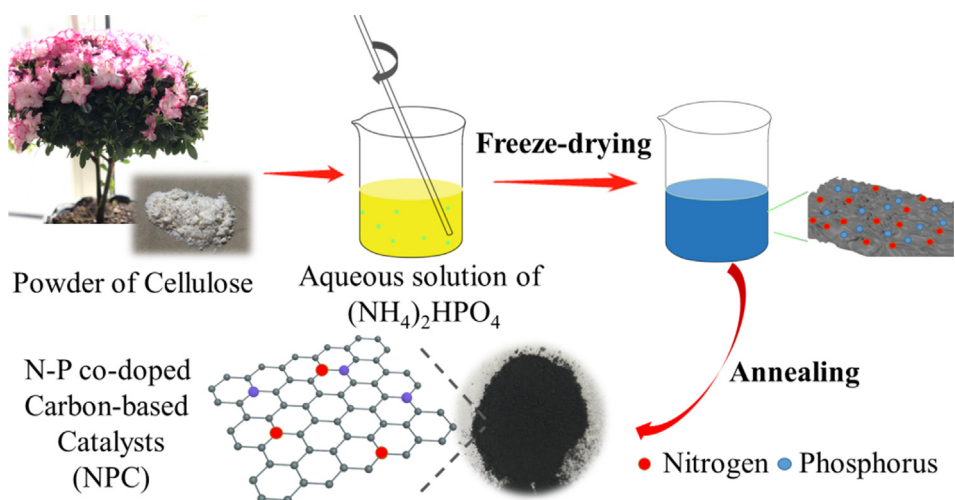

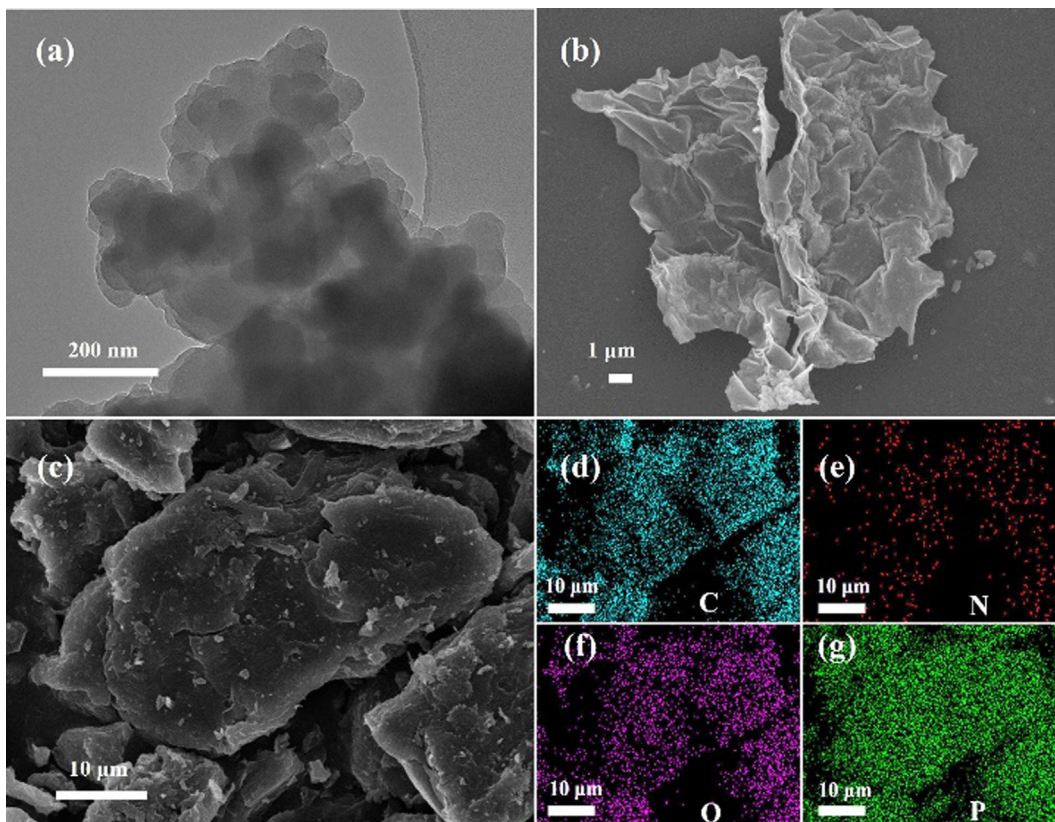**Fig. 1.** Schematic of the preparation process of NPC.

Fig. 2. (a) TEM image, (b) SEM image, and (c) SEM corresponding EDS mapping of (d) carbon, (e) nitrogen, (f) oxygen, (g) phosphorus elementals of NPC.
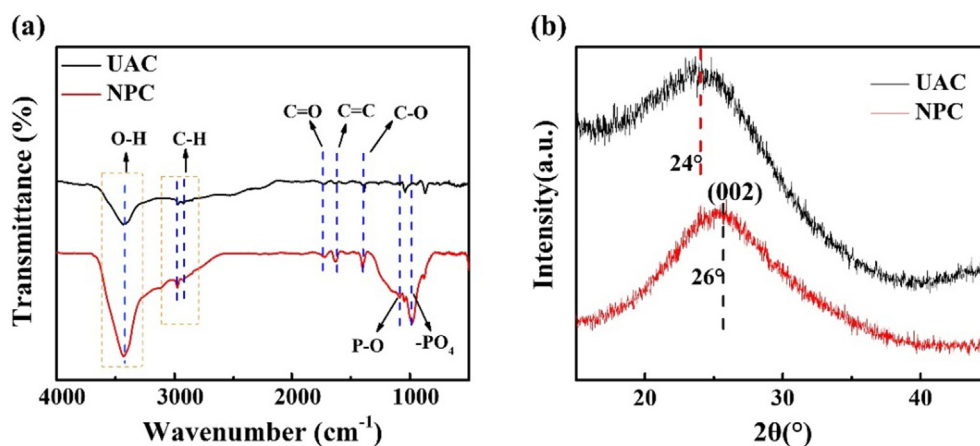

Fig. 3. (a) FTIR spectrum of NPC and UAC, (b) XRD patterns of NPC and UAC.

$$\ln\left(\frac{A}{A_0}\right) = \ln\left(\frac{C}{C_0}\right) = k_{app}t \qquad (2)$$

where A and A_0 are the absorbance of p-NP at 400 nm at time of t, and 0 min, respectively, C and C_0 are the corresponded concentration of p-NP obtained from A and A_0.

For a first-order reaction, the activation energy reflects the difficulty of the chemical reaction happens, while activation enthalpy (ΔH) and entropy (ΔS) are important state parameters in thermodynamics that characterize the energy and chaos of a material system. Thus, the reduction of p-NP to p-AP by NPC catalyst was conducted under several different reaction temperature (303 K, 313 K, 323 K, and 333 K) to obtain thermodynamic parameters

according to Arrhenius equations (Eq. (3)) and Eyring equation (Eq. (4)).

$$\ln k_{app} = \ln A - \frac{E_a}{RT} \qquad (3)$$

$$\ln\left(\frac{k_{app}}{T}\right) = \frac{\Delta S}{R} - \frac{\Delta H}{R}\left(\frac{1}{T}\right) + \ln\left(\frac{k_B}{\hbar}\right) \qquad (4)$$

where A is the pre-exponential factor, E_a is apparent activation energy, T is thermodynamic temperature, R is the molar gas constant ($R = 8.314$ J K^{-1} mol^{-1}). Besides, k_B ($k_B = 1.38 \times 10^{-23}$ J/K), and $\hbar$ ($\hbar = 6.63 \times 10^{-34}$ J) represent Boltzmann, and Planck constants, respectively.
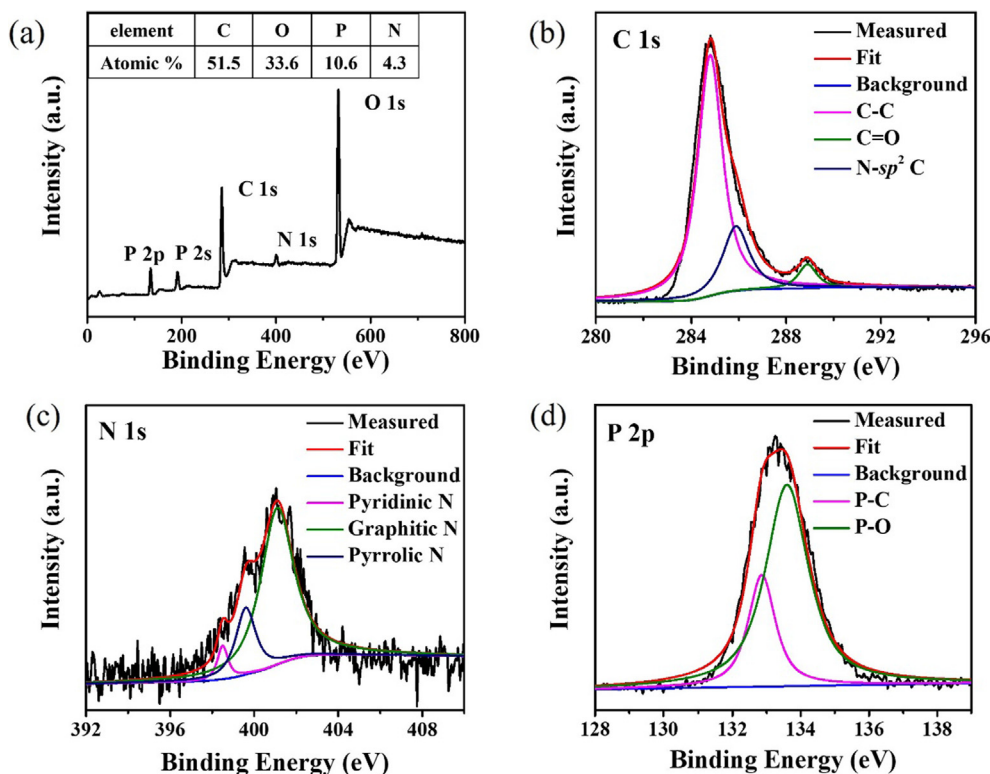
Fig. 4. (a) XPS spectrum of NPC sample and the corresponding core-level spectrum of (b) C 1s, (c) N 1s, and (d) P 2p.
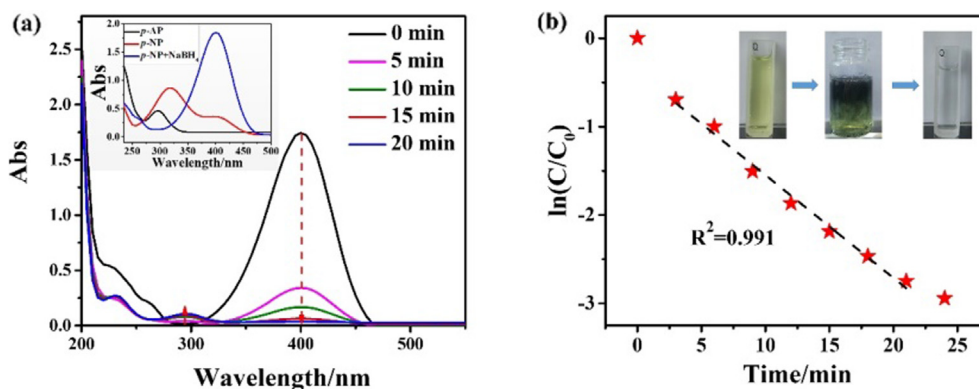

Fig. 5. (a) Catalytic reduction of NaBH$_4$/p-NP by NPC for various times, with inset showing the standard UV/vis characteristic peaks of p-NP, p-NP with NaBH$_4$, and p-AP, (b) The linear fit of ln (C/C$_0$) versus time. (Reaction conditions: room temperature, 30 mg NPC powder, 1.5 mmol NaBH$_4$ powder 30 mL p-NP solution (0.5 mM)).

Fig. 6a shows the relationship between ln(C/C$_0$) and times at different reaction temperatures. Apparently, the linear slope increased as temperature goes up, indicating the reaction proceeds at a higher rate when the temperature is higher. As a typical surface reaction, the transfer rate of p-NP is related to effective collision chance between reactant and catalyst. In this condition, a higher temperature of the system can cause more intense of the molecular motion, which will increase the number of effective collisions, and then resulting in a faster reaction rate. Fig. 6b displays the ln(k$_{app}$) and ln(k$_{app}$/T) versus 1000/T. According to Eqs. (3) and (4), the E$_a$ of reduction of p-NP by NPC catalyst can be calculated as 21.55 kJ mol^{-1}, which is lower than the value of previously reported SG catalyst (E$_a$ = 24.21 kJ mol^{-1}) [22], indicating the NPC can accelerate the reaction rate at extremely low reaction energy barrier. In addition, the values of ΔS and ΔH are calculated as −203.18 kJ mol^{-1} K^{-1}, and 18.91 kJ mol^{-1}, respectively.

In a heterogeneous catalytic reaction, turn over frequency (TOF), defined as the number of the molecules of substrate converted to products by unit mass of catalyst, is used to assess the catalytic activity of the catalyst [42]. The TOF (mmol p-NP/(mg catalyst min)) value of the reduction of p-NP catalyzed by NPC is calculated as 2×10^{-5} at room temperature, which is comparable to the TOF values of previously reported noble metal supported carbon-based catalysts and conventional graphene-based catalysts, such as nitrogen-doped graphene (6.65×10^{-5}) [43], Au/graphene (2.2×10^{-5}) [44], CMF@PDA/Pd (8.13×10^{-5}) [45], calcium alginate/Ag (1×10^{-5}) [46], and so on [47,48] (Table 1). It should also be noted that the raw material of NPC prepared in this work is one of the most abundant solid by-products of agriculture and forestry industry, which is widely available carbon source and an rich polysaccharide in nature.
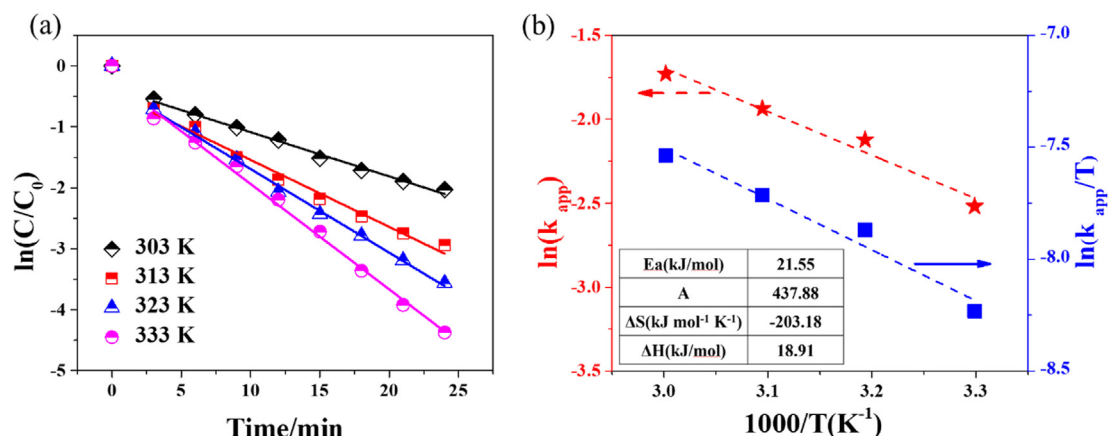
Fig. 6. (a) $\ln(C/C_0)$ versus time under different reaction temperature. (b) $\ln(k_{app})$ and $\ln(k_{app}/T)$ versus $1000/T$.

Table 1
Catalytic activity comparison of different metal-based and metal-free carbon-based catalysts for hydrogenation of p-NP.

Catalyst	$m_{catalyst}$ (mg)	Molars of p-NP (mmol)	Reaction time (min)	TOF (mmol/mg min)	Ref.
Nitrogen-doped graphene	0.137	1.76×10^{-4}	21	6.65×10^{-5}	[43]
Au/graphene	1.06	2.8×10^{-4}	12	2.2×10^{-5}	[44]
pH-mediated graphene	2.5	5×10^{-4}	60	3.33×10^{-6}	[47]
CMF@PDA/Pd	492	1×10^{-2}	0.25	8.13×10^{-5}	[45]
Au@C	5.0	3×10^{-4}	5	1.2×10^{-5}	[48]
Calcium alginate/Ag	3.0	2.5×10^{-4}	8	1×10^{-5}	[46]
NPC	30	1.5×10^{-2}	25	2×10^{-5}	This work

Furthermore, durability is one of the most important indicators for evaluating catalysts' performance. In this work, the catalyst powder was obtained after each reaction and then used for the next cycle test. Fig. 7a shows the catalytic performance variations during the continuous four cycles and Fig. 7b displays the ratio of k_{app} for each cycle to the first time. Apparently, the rate performance can still maintain over 90% after 4 cycles, which indicates the significant durability of the NPC catalyst.

In fact, the mechanism of metal-based or metal supported carbon-based catalysts catalytic p-NP/NaBH$_4$ has been reported in many literatures. However, the process of hydrogenation of p-NP by cellulose-derived carbon-based catalyst is rarely explored, especially nitrogen-phosphorus co-doped carbon material. Herein, we proposed reaction routes of reducing p-NP/NaBH$_4$ by NPC catalyst (Fig. 8). Firstly, NaBH$_4$ is hydrolyzed in water to form borohydride ions, which are then passed to the NPC carbon skeleton. At the same time, the p-NP molecules diffuse and adsorbed on the

active sites on the surface of the NPC carbon skeleton, such as the exposed N, P defect sites and large π bonds. Finally, p-NP is converted into p-AP, which is then desorbed from the active site. The nitrogen and phosphorus elemental are co-doped in the graphite carbon skeleton, causing synergistic effects between C, N, O, and P electronic properties, creating a large number of active sites, which greatly improves the catalytic performance of NPC. This work will provide a good research prospect for the application of cellulose materials in organic catalytic reactions.

In order to further study the catalytic reduction performance of NPC, the configuration of NPC adsorption p-NP was optimized by DFT (Fig. 9). Seven possible doping types of the NPC were explored. Fig. 9b–h shows the morphology of seven doped materials and the configuration of the adsorbed p-NP and the corresponding bond length. The OH bond length of p-NP before adsorbed (Fig. 8(a)), adsorbed by C$_3$P (Fig. 9b), and C$_3$PO (Fig. 9e) is 0.974 Å, 0.981 Å, and 1.001 Å, respectively, which means that C$_3$P and C$_3$PO have a
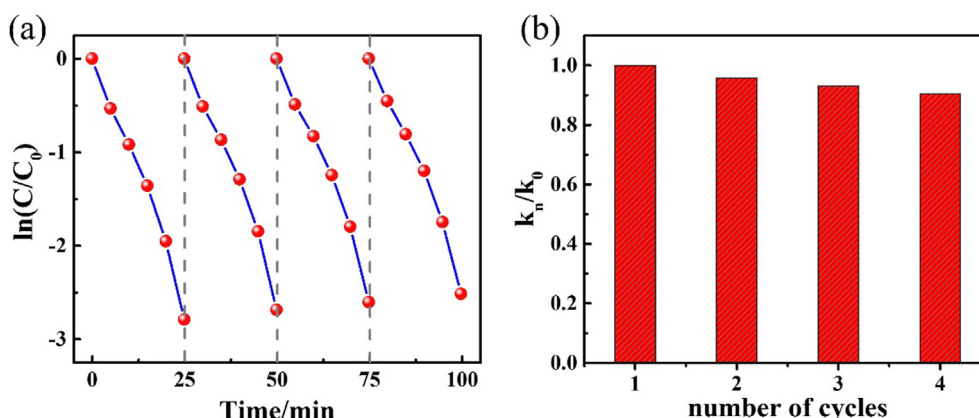

Fig. 7. (a) The curves of $\ln(C/C_0)$ as a function of time for four cycles (b) The ratio of k_{app} for each cycle to the first cycle.
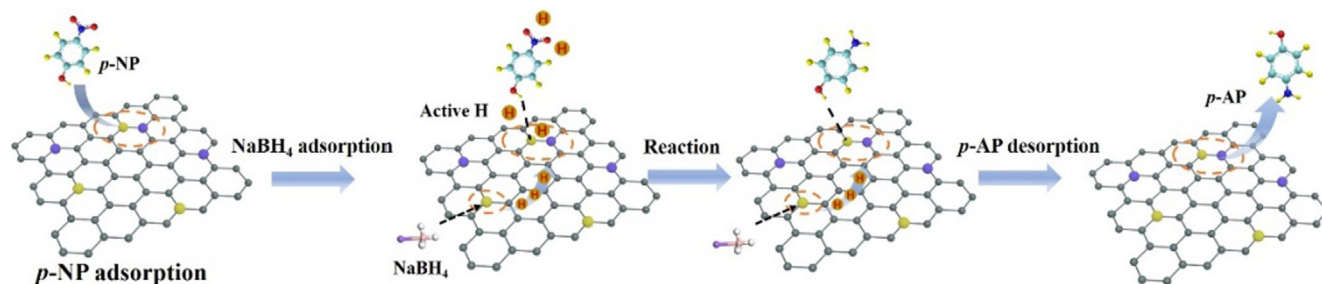
Fig. 8. Proposed reaction mechanism of *p*-NP reduction by cellulose-derived metal-free catalyst.
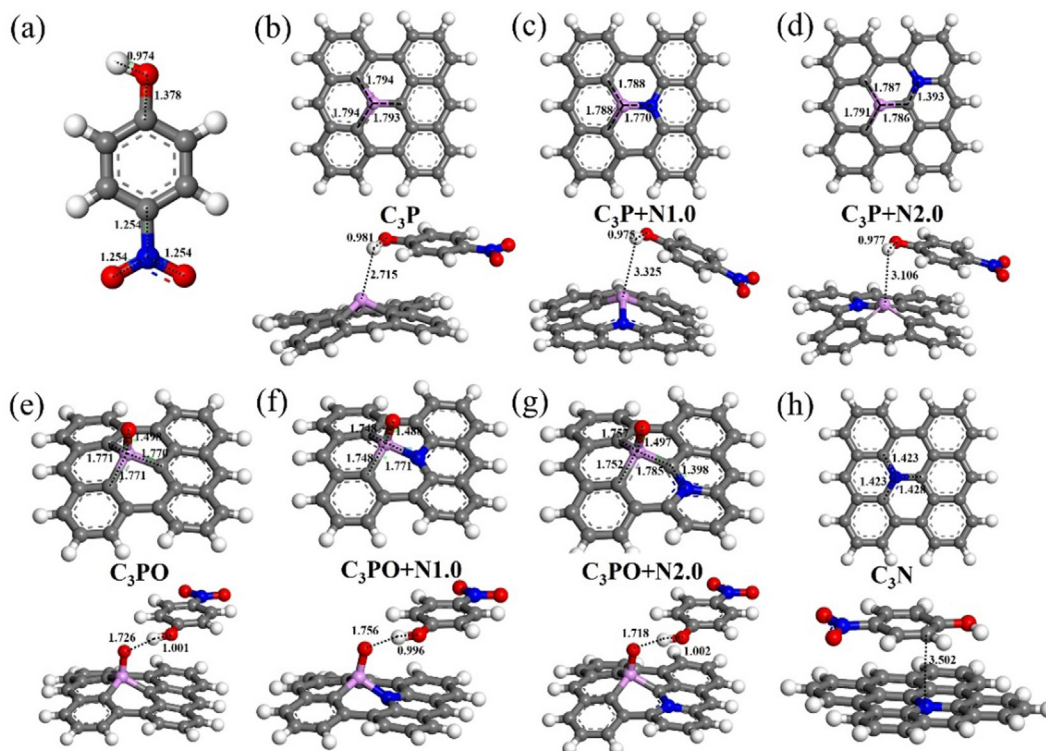

Fig. 9. (a) The *p*-NP molecular model. The calculated structures of (b) P-doped graphite carbon skeleton, (c) N, P co-doped (in adjacent positions) graphite carbon skeleton, (d) N and P co-doped (separated by one carbon atom) graphite carbon skeleton, (e) O=P-doped graphite carbon skeleton, (f) N and O=P co-doped (in the ortho-position) graphite carbon skeleton, (g) N and O=P co-doped(in the meta-position) graphite carbon skeleton, (h) N-doped graphite carbon skeleton.

strong adsorption force on the OH group of *p*-NP, resulting in elongation of the OH bond. In addition, the O atom in the adsorption structure of C_3PO is 1.726 Å away from the H atom of OH in *p*-NP, while that for P atom in adsorption structure of C_3P is 2.715 Å, which means that the adsorption force of C_3PO on *p*-NP is stronger than that of C_3P. Table 2 shows the E_{ads} of these adsorption structures and the charge of the N, P, and O elements. Among them, the absolute value of the E_{ads} of $C_3PO + N2.0$ is 0.9254 eV, which means it has the strongest adsorption effect on *p*-NP, confirming the catalytic performance of nitrogen and phosphorus

co-doped material is superior to nitrogen or phosphorus mono-doped. This conclusion is consistent with the previous literatures [31,49].

As reported in the previous literature [19,50], the catalytic properties of non-metallic atom (B, N, P and S)-doped graphitic carbon skeleton are closely related to the electron orbital distribution on the carbon skeleton. Therefore, the partial density of states (PDOS) further explains why the catalytic performance of $C_3PO + N2.0$ is better than C_3P. Fig. 10 shows PDOS of $C_3PO + N2.0$ and C_3P, respectively. The PDOS of the remaining

Table 2
The E_{ads} of *p*-NP absorbed on seven different sites and the electric charge of N, P, and O elements in different materials.

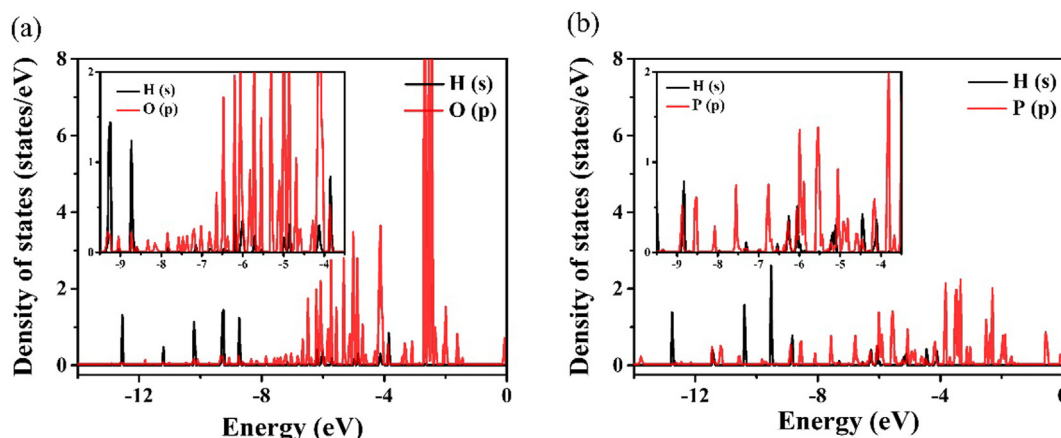| Structure		C_3N	C_3P	$C_3P+N1.0$	$C_3P+N2.0$	C_3PO	$C_3PO+N1.0$	$C_3PO+N2.0$	*p*-NP
E_{ads}		−0.612	−0.453	−0.456	−0.441	−0.904	−0.893	−0.925	–
Electric charge	N	−1.176	–	−1.392	−1.18	–	−1.397	−1.183	0.308
	P	–	1.60	1.686	1.605	3.045	3.091	3.044	–
	O	–	–	–	–	−1.394	−1.404	−1.398	−1.145
									−0.457
									−0.449

Fig. 10. (a) Partial density of states (PDOS) of $C_3PO + N2.0$, (b) PDOS of C_3P.

materials is shown in Fig. S4. Fig. 10a shows the overlap of the s orbital electrons of the H atom in *p*-NP and the p orbital electrons of the O atom in $C_3PO + N2.0$. Fig. 10b shows the overlap between the s orbital electrons of the H atom in *p*-NP and the p orbital electrons of the P atom in C_3P. It can be seen that the orbital electron coincidence portion of $C_3PO + N2.0$ is more than C_3P. This means that the adsorption capacity of $C_3PO + N2.0$ for *p*-NP is stronger than that of C_3P, which is consistent with the E_{ads} by DFT.

4. Conclusions

In summary, we reported a green and economical method for the preparation of NPC catalysts with α-cellulose crystallite as carbon source and $(NH_4)_2HPO_4$ as both nitrogen and phosphorus source. The NPC presented flake-like morphology with N and P elemental doping level of 4.3 atom% and 10.66 atom%. The NPC can be used as efficient metal-free catalyst for the reduction of *p*-NP. The TOF (mmol *p*-NP/(mg catalyst min)) of the reduced *p*-NP is 2×10^{-5}, which is comparable to those of noble metal-based catalysts and conventional graphene-based catalysts. The activation energy (E_a) of the reduction of *p*-NP by NPC was measured as 21.55 kJ mol^{-1} at several different temperature conditions. The reaction mechanism is proposed according to both thermodynamic studies and DFT calculations. Moreover, the DFT calculation reveals the adsorption activation mechanism of the cellulose-derived N/P-doped metal-free carbon material for the catalytic reduction of *p*-NP, and points out that the main source of the catalytic activity of the metal-free carbon material prepared in this work is nitrogen and phosphorus co-doped. These findings broaden the range of applications of cellulose-derived carbon-based metal-free catalysts in organic catalysis.

CRediT authorship contribution statement

Xiong Xie: Investigation, Data curation, Writing - original draft. **Jie Shi:** Validation, Software. **Yuan Pu:** Supervision, Writing - review & editing. **Zhiyong Wang:** Validation, Data curation. **Liang-Liang Zhang:** Writing - review & editing. **Jie-Xin Wang:** Writing - review & editing. **Dan Wang:** Conceptualization, Methodology, Writing - review & editing.

Declaration of Competing Interest

The authors declare that they have no known competing financial interests or personal relationships that could have appeared to influence the work reported in this paper.

Acknowledgements

Appendix A. Supplementary material

Supplementary data to this article can be found online at https://doi.org/10.1016/j.jcis.2020.03.035.

References

[1] C. Zhang, S. Govindaraju, K. Giribabu, Y.S. Huh, K. Yun, AgNWs-PANI nanocomposite based electrochemical sensor for detection of 4-nitrophenol, Sens. Actuat. B – Chem. 252 (2017) 616–623.

[2] P. Wiench, B. Grzyb, Z. González, R. Menéndez, B. Handke, G. Gryglewicz, pH robust electrochemical detection of 4-nitrophenol on a reduced graphene oxide modified glassy carbon electrode, J. Electroanal. Chem. 787 (2017) 80–87.

[3] X. Gao, H. Zhao, Y. Liu, Z. Ren, C. Lin, J. Tao, Y. Zhai, Facile synthesis of PdNiP/ Reduced graphene oxide nanocomposites for catalytic reduction of 4-nitrophenol, Mater. Chem. Phys. 222 (2019) 391–397.

[4] J. Liu, X. Yan, L. Wang, L. Kong, P. Jian, Three-dimensional nitrogen-doped graphene foam as metal-free catalyst for the hydrogenation reduction of p-nitrophenol, J. Colloid Interf. Sci. 497 (2017) 102–107.

[5] G. Wu, X. Liang, L. Zhang, Z. Tang, M. Al-Mamun, H. Zhao, X. Su, Fabrication of highly stable metal oxide hollow nanospheres and their catalytic activity toward 4-nitrophenol reduction, ACS Appl. Mater. Inter. 9 (2017) 18207–18214.

[6] Z. Yan, L. Fu, X. Zuo, H. Yang, Green assembly of stable and uniform silver nanoparticles on 2D silica nanosheets for catalytic reduction of 4-nitrophenol, Appl. Catal. B-Environ. 226 (2018) 23–30.

[7] J. Mohanta, S. Satapathy, S. Si, Porous silica-coated gold nanorods: a highly active catalyst for the reduction of 4-nitrophenol, ChemPhysChem 17 (2016) 364–368.

[8] X. Duan, M. Xiao, S. Liang, Z. Zhang, Y. Zeng, J. Xi, S. Wang, Ultrafine palladium nanoparticles supported on nitrogen-doped carbon microtubes as a high-performance organocatalyst, Carbon 119 (2017) 326–331.

[9] H. Park, D.A. Reddy, Y. Kim, S. Lee, R. Ma, M. Lim, T.K. Kim, Hydrogenation of 4-nitrophenol to 4-aminophenol at room temperature: boosting palladium nanocrystals efficiency by coupling with copper via liquid phase pulsed laser ablation, Appl. Surf. Sci. 401 (2017) 314–322.

[10] Y. Wang, Q. Li, P. Zhang, D. O'Connor, R.S. Varma, M. Yu, D. Hou, One-pot green synthesis of bimetallic hollow palladium-platinum nanotubes for enhanced catalytic reduction of p-nitrophenol, J. Colloid Interf. Sci. 539 (2019) 161–167.

[11] Y. Long, Y. Liu, Z. Zhao, S. Luo, W. Wu, L. Wu, H. Wen, R.Q. Wang, J. Ma, Distinctive morphology effects of porous-spherical/yolk-shell/hollow Pd-nitrogen-doped-carbon spheres catalyst for catalytic reduction of 4-nitrophenol, J. Colloid Interf. Sci. 496 (2017) 465–473.

[12] Y. Yang, D. Zeng, S. Shao, S. Hao, G. Zhu, B. Liu, Construction of core-shell mesoporous carbon nanofiber@nickel cobaltite nanostructures as highly efficient catalysts towards 4-nitrophenol reduction, J. Colloid Interf. Sci. 538 (2019) 377–386.

[13] J. Shan, X. Sun, S. Zheng, T. Wang, X. Zhang, G. Li, Graphitic n-dominated nitrogen-doped carbon nanotubes as efficient metal-free catalysts for hydrogenation of nitroarenes, Carbon 146 (2019) 60–69.

[14] K. Chen, D. Cheng, C. Peng, D. Wang, J. Zhang, Green catalytic engineering: a powerful tool for sustainable development in chemical industry, Front. Chem. Sci. Eng. 12 (2018) 835–837.

[15] Z. Wang, Y. Pu, D. Wang, J.-X. Wang, J.-F. Chen, Recent advances on metal-free graphene-based catalysts for the production of industrial chemicals, Front. Chem. Sci. Eng. 12 (2018) 855–866.

[16] J.P. Paraknowitsch, A. Thomas, Doping carbons beyond nitrogen: an overview of advanced heteroatom doped carbons with boron, sulphur and phosphorus for energy applications, Energ. Environ. Sci. 6 (2013) 2839–2855.

[17] X. Duan, H. Sun, S. Wang, Metal-free carbocatalysis in advanced oxidation reactions, Acc. Chem. Res. 51 (2018) 678–687.

[18] C. Han, Z. Chen, Adsorption properties of O_2 on the unequal amounts of binary co-doped graphene by B/N and P/N: a density functional theory study, Appl. Surf. Sci. 471 (2019) 445–454.

[19] Z. Zhang, S. Yang, H. Li, Y. Zan, X. Li, Y. Zhu, M. Dou, F. Wang, Sustainable carbonaceous materials derived from biomass as metal-free electrocatalysts, Adv. Mater. 31 (2019) 1805718.

[20] X. Zhao, S. Wang, Q. Wu, Nitrogen and phosphorus dual-doped hierarchical porous carbon with excellent supercapacitance performance, Electrochim. Acta 247 (2017) 1140–1146.

[21] Q. Liu, Y. Zhou, S. Chen, Z. Wang, H. Hou, F. Zhao, Cellulose-derived nitrogen and phosphorus dual-doped carbon as high performance oxygen reduction catalyst in microbial fuel cell, J. Power Sources 273 (2015) 1189–1193.

[22] Z. Wang, R. Su, D. Wang, J. Shi, J.-X. Wang, Y. Pu, J.-F. Chen, Sulfurized graphene as efficient metal-free catalysts for reduction of 4-nitrophenol to 4-aminophenol, Ind. Eng. Chem. Res. 56 (2017) 13610–13617.

[23] Y. Pu, F. Cai, D. Wang, Y. Li, X. Chen, A.G. Maimouna, Z. Wu, X. Wen, J.-F. Chen, N.R. Foster, Solubility of bicalutamide, megestrol acetate, prednisolone, beclomethasone dipropionate, and clarithromycin in subcritical water at different temperatures from 383.15 to 443.15 K, J. Chem. Eng. Data 62 (2017) 1139–1145.

[24] G. Kresse, J. Furthmüller, Efficient iterative schemes for ab initio total-energy calculations using a plane-wave basis set, Phys. Rev. B 54 (1996) 11169–11186.

[25] J.P. Perdew, K. Burke, M. Ernzerhof, Generalized gradient approximation made simple, Phys. Rev. Lett. 77 (1996) 3865–3868.

[26] Y. Zhang, W. Yang, Comment on "Generalized gradient approximation made simple", Phys. Rev. Lett. 80 (1998) 890.

[27] D. Vanderbilt, Optimally smooth norm-conserving pseudopotentials, Phys. Rev. B 32 (1985) 8412–8415.

[28] M. Dion, H. Rydberg, E. Schröder, D.C. Langreth, B.I. Lundqvist, Van der waals density functional for general geometries, Phys. Rev. Lett. 92 (2004) 246401.

[29] K. Sun, S. Yu, Z. Hu, Z. Li, G. Lei, Q. Xiao, Y. Ding, Oxygen-containing hierarchically porous carbon materials derived from wild jujube pit for high-performance supercapacitor, Electrochim. Acta 231 (2017) 417–428.

[30] Z. Wang, Y. Tan, Y. Yang, X. Zhao, Y. Liu, L. Niu, B. Tichnell, L. Kong, L. Kang, Z. Liu, F. Ran, Pomelo peels-derived porous activated carbon microsheets dual-doped with nitrogen and phosphorus for high performance electrochemical capacitors, J. Power Sources 378 (2018) 499–510.

[31] J. Xi, Q. Wang, J. Liu, L. Huan, Z. He, Y. Qiu, J. Zhang, C. Tang, J. Xiao, S. Wang, N, P-dual-doped multilayer graphene as an efficient carbocatalyst for nitroarene reduction: a mechanistic study of metal-free catalysis, J. Catal. 359 (2018) 233–241.

[32] N. Wang, C. Wang, L. He, Y. Wang, W. Hu, S. Komarneni, Incomplete phase separation strategy to synthesize P/N co-doped porous carbon with interconnected structure for asymmetric supercapacitors with ultra-high power density, Electrochim. Acta 298 (2019) 717–725.

[33] T. Wang, J. Tang, X. Fan, J. Zhou, H. Xue, H. Guo, J. He, The oriented growth of tungsten oxide in ordered mesoporous carbon and their electrochemical performance, Nanoscale 6 (2014) 5359–5371.

[34] L. Song, T. Wang, Y. Ma, H. Xue, H. Guo, X. Fan, W. Xia, H. Gong, J. He, Functional species encapsulated in nitrogen-doped porous carbon as a highly efficient catalyst for the oxygen reduction reaction, Chemistry 23 (2017) 3398–3405.

[35] M. Wu, J. Zhang, B.-B. He, H.-W. Wang, R. Wang, Y.-S. Gong, In-situ construction of coral-like porous P-doped g-C3N4 tubes with hybrid 1D/2D architecture and high efficient photocatalytic hydrogen evolution, Appl. Catal. B-Environ. 241 (2019) 159–166.

[36] R. Vinoth, S.G. Babu, D. Bahnemann, B. Neppolian, Nitrogen doped reduced graphene oxide hybrid metal free catalyst for effective reduction of 4-nitrophenol, Sci. Adv. Mater. 7 (2015) 1443–1449.

[37] T. Huang, Y. Fu, Q. Peng, C. Yu, J. Zhu, A. Yu, X. Wang, Catalytic hydrogenation of p-nitrophenol using a metal-free catalyst of porous crimped graphitic carbon nitride, Appl. Surf. Sci. 480 (2019) 888–895.

[38] F. Yang, X. Fan, C. Wang, W. Yang, L. Hou, X. Xu, A. Feng, S. Dong, K. Chen, Y. Wang, Y. Li, P-doped nanomesh graphene with high-surface-area as an efficient metal-free catalyst for aerobic oxidative coupling of amines, Carbon 121 (2017) 443–451.

[39] Z. Wang, Y. Pu, D. Wang, J. Shi, J.-X. Wang, J.-F. Chen, 3D-foam-structured nitrogen-doped graphene-Ni catalyst for highly efficient nitrobenzene reduction, AIChE J. 64 (2018) 1330–1338.

[40] D.S. Yang, D. Bhattacharjya, S. Inamdar, J. Park, J.S. Yu, Phosphorus-doped ordered mesoporous carbons with different lengths as efficient metal-free electrocatalysts for oxygen reduction reaction in alkaline media, J. Am. Chem. Soc. 134 (2012) 16127–16130.

[41] Z. Zhao, X. Ma, X. Wang, Y. Ma, C. Liu, H. Hang, Y. Zhang, Y. Du, W. Ye, Synthesis of amorphous PdP nanoparticles supported on carbon nanospheres for 4-nitrophenol reduction in environmental applications, Appl. Surf. Sci. 457 (2018) 1009–1017.

[42] M. Bano, D. Ahirwar, M. Thomas, G.A. Naikoo, M.U.-D. Sheikn, F. Khan, Hierarchical synthesis of silver monoliths and their efficient catalytic activity for the reduction of 4-nitrophenol to 4-aminophenol, New J. Chem. 40 (2016) 6787–6795.

[43] X.-K. Kong, Z.-Y. Sun, M. Chen, C.-L. Chen, Q.-W. Chen, Metal-free catalytic reduction of 4-nitrophenol to 4-aminophenol by N-doped graphene, Energ. Environ. Sci. 6 (2013) 3260–3266.

[44] J. Li, C.-Y. Liu, Y. Liu, Au/graphene hydrogel: synthesis, characterization and its use for catalytic reduction of 4-nitrophenol, J. Mater. Chem. 22 (2012) 8426–8430.

[45] J. Xi, J. Xiao, F. Xiao, Y. Jin, Y. Dong, F. Jing, S. Wang, Mussel-inspired functionalization of cotton for nano-catalyst support and its application in a fixed-bed system with high performance, Sci. Rep. 6 (2016) 21904.

[46] S. Sandip, A. Pal, S. Kundu, S. Basu, T. Pal, Photochemical green synthesis of calcium-alginate-stabilized Ag and Au nanoparticles and their catalytic application to 4-nitrophenol reduction, Langmuir 4 (2010) 2885–2893.

[47] H. Hu, X. Wang, D. Miao, Y. Wang, C. Lai, Y. Guo, W. Wang, J.H. Xin, H. Hu, A pH-mediated enhancement of the graphene carbocatalyst activity for the reduction of 4-nitrophenol, Chem. Commun. 51 (2015) 16699–16702.

[48] R. Liu, S.M. Mahurin, C. Li, R.R. Unocic, J.C. Idrobo, H. Gao, S.J. Pennycook, S. Dai, Dopamine as a Carbon Source: the controlled synthesis of hollow carbon spheres and yolk-structured carbon nanocomposites, Angew. Chem. Int. Ed. 50 (2011) 6799–6802.

[49] K. Li, J. Liu, J. Li, Z. Wan, Effects of N mono- and N/P dual-doping on H_2O_2, OH generation, and MB electrochemical degradation efficiency of activated carbon fiber electrodes, Chemosphere 193 (2018) 800–810.

[50] X. Li, X. Duan, C. Han, X. Fan, Y. Li, F. Zhang, G. Zhang, W. Peng, S. Wang, Chemical activation of nitrogen and sulfur co-doped graphene as defect-rich carbocatalyst for electrochemical water splitting, Carbon 148 (2019) 540–549.